Title
Transcatheter intra-arterial perfusion (TRIP)-MRI biomarkers help detect immediate response to irreversible electroporation of rabbit VX2 liver tumor

Journal
Magnetic Resonance in Medicine, 84(1)

ISSN
0740-3194

Authors
Figini, Matteo
Zhou, Kang
Pan, Liang
et al.

Publication Date
2020-07-01

DOI
10.1002/mrm.28104

Peer reviewed

HHS Public Access

Author manuscript

Magn Reson Med. Author manuscript; available in PMC 2021 July 01.

Published in final edited form as:

Magn Reson Med. 2020 July ; 84(1): 365–374. doi:10.1002/mrm.28104.

Transcatheter Intra-arterial Perfusion (TRIP)-MRI Biomarkers Help Detect Immediate Response to Irreversible Electroporation of Rabbit VX2 Liver Tumor

Matteo Figini[1,*], **Kang Zhou**[1,2,*], **Liang Pan**[1,3], **Chong Sun**[1,4], **Bin Wang**[1,5], **Su Hu**[1,6], **Jia Yang**[1], **Junjie Shangguan**[1], **Aydin Eresen**[1], **Yury Velichko**[1,7], **Vahid Yaghmai**[1,7], **Zhuoli Zhang**[1,7]

[1]Department of Radiology, Feinberg School of Medicine, Northwestern University, Chicago, IL, USA

[2]Department of Radiology, Peking Union Medical College Hospital, Chinese Academy of Medical Sciences, Beijing, China

[3]Department of Radiology, The Third Affiliated Hospital of Suzhou University, Changzhou, Jiangsu, China

[4]Department of Orthopaedics, The Affiliated Hospital of Qingdao University, Qingdao, Shandong, China

[5]Department of General Surgery, Nanfang Hospital, Southern Medical University, Guangdong provincial Engineering Technology Research Center of Minimally Invasive Surgery, Guangzhou, China

[6]Department of Radiology, The First Affiliated Hospital of Soochow University, Suzhou, Jiangsu, China

[7]Robert H. Lurie Comprehensive Cancer Center, Northwestern University, Chicago, IL, USA

Abstract

Purpose: Irreversible electroporation (IRE) is a nonthermal tissue ablation technique that represents a promising treatment option for unresectable liver tumors, but the effectively treated zone cannot be reliably predicted. We investigate the potential benefit of transcatheter intra-arterial perfusion (TRIP)-MRI for the early noninvasive differentiation of IRE zone from surrounding reversibly electroporated (RE) zone.

Methods: Seventeen rabbits with VX2 liver tumors were scanned with morphological and contrast-enhanced MRI sequences about 30 minutes after IRE tumor ablation. Quantitative TRIP-MRI perfusion parameters were evaluated in IRE zone and RE zone, defined according to histology. MRI and histology results were compared among zones using Wilcoxon rank-sum tests and correlations were evaluated by Pearson's correlation coefficient.

Corresponding author: Zhuoli Zhang, Northwestern University, Department of Radiology, 737 N Michigan Ave, 16th Floor, Chicago, IL 60611, USA, Phone: (312)695-5753, Fax: (312)926-5991, zhuoli-zhang@northwestern.edu.

*These authors contributed equally to this work

Results: There were significant differences in area under the curve, time-to-peak, maximum and late enhancement, wash-in and wash-out rates in the tumor IRE zones compared to the boundary tumor RE zones and untreated tumors. Histology showed significantly fewer tumor cells, microvessels and significantly more apoptosis in tumor IRE zones compared to tumor RE zones (−51%, −66% and +185% respectively) and untreated tumors (−60%, −67% and +228% respectively). A strong correlation was observed between MRI and histology measurements of IRE zones (r = 0.948) and RE zones (r = 0.951).

Conclusion: TRIP-MRI demonstrated the potential to detect immediate perfusion changes following IRE liver tumor ablation and effectively differentiate the IRE zone from the surrounding tumor RE zone.

Keywords

Irreversible Electroporation; Transcatheter intra-arterial perfusion (TRIP)-MRI; Liver tumors; reversibly electroporated zone; irreversibly electroporated zone; Rabbit

Introduction

Patients with unresectable hepatocellular carcinoma (HCC) or metastatic liver tumors commonly undergo thermal ablation procedures that involve cooling or heating of targeted tumor tissues with percutaneous probes. While thermal ablation has gained widespread acceptance, it has also demonstrated several critical drawbacks that can limit its efficacy in the clinical setting.[1–4] Irreversible electroporation (IRE) is a nonthermal tissue ablation technique that causes cell death in tumor tissue while preserving the extracellular matrix and inducing minimal inflammation, which makes it a promising treatment for unresectable liver tumors.[5] IRE involves the application of strong electric pules to the target tumor creating a central ablation zone containing complete necrotic tissue (defined as irreversibly electroporated zone, IRE zone) from a surrounding zone containing viable tissue (defined as reversibly electroporated zone, RE zone).[6–11]

The main limitation of IRE ablation is the uncertainty in the prediction of effectively IRE zone and RE zone, which depends on the treatment protocol and features of the tissue.[12–14] It would be critical to have an early noninvasive tool to distinguish the tumor IRE zone from the surrounding tumor RE zone or/and normal liver tissue immediately after treatment. This would allow retreatment or other interventions to be timely performed to minimize the likelihood of recurrence while preserving the vital healthy surrounding tissues.

Noninvasive imaging plays an important role in IRE studies, e.g. preoperative planning, intraoperative guidance, assessment of treatment outcome and complications. MRI demonstrates potential superiority to the commonly used US and CT for the depiction and characterization of the ablated area and is increasingly being used.[15] However, the utility of advanced and quantitative MRI techniques has not been thoroughly investigated.[16]

TRIP-MRI is a technique evaluating the perfusion features of the tissue after direct injection of the contrast agent into the tumor tissue of interest through an intra-arterial catheter. Continuous iterative volumetric imaging over time of TRIP-MRI incorporates the benefits of

high spatial and temporal resolution with intraprocedural monitoring for objective perfusion quantification.[17] It has been previously shown to successfully characterize perfusion changes after chemoembolization and radiofrequency ablation of liver tumors.[18,19]

The purpose of this study is to investigate the potential benefit of TRIP-MRI for the early noninvasive differentiation of IRE zone and surrounding tumor RE zone.

Methods

Animal model

All animal methods are approved by the Institutional Animal Care and Use Committee of Northwestern University. Nineteen rabbits weighing 3.0-3.5 kg (New Zealand White, Covance, Princeton, NJ) were used for this study, i.e. two donor rabbits for VX2 incubation and 17 rabbits for the MRI and histology experiments. In brief, basic anesthesia was induced by intramuscular injection of ketamine (100 mg/kg) and xylazine (5 mg/kg) and maintained by inhalation of isoflurane (2-3 % in oxygen, 3 L/min). VX2 tumor cells were implanted in the hind limbs of donor rabbits and harvested when tumor size is reached approximately 3 cm in diameter. Donor tumor fragments (around 1 mm^3) were implanted into the liver left lobe of the other 17 rabbits using a biopsy needle under percutaneous ultrasound-guidance. Tumors were allowed to grow for 7-10 days until the longest diameter reached at least 10 mm by MRI measurement. All the rabbits developed at least one tumor and 7 out of 17 rabbits had a second tumor that was not treated but used as an internal control.

Digital subtraction angiography (DSA)

About two weeks after implantation, when the tumors were grown to a diameter between 1 and 1.5 cm, the rabbits were anesthetized with an injection of 100 mg/kg ketamine and 5 mg/kg xylazine. X-ray DSA-guided hepatic artery catheterizations were performed using a C-arm unit (Powermobil; Siemens Medical Solutions, Erlangen, Germany). The femoral artery was accessed through surgical cut-down; an introducer needle was inserted and exchanged with a 3-F introducer sheath (Check-Flo; Cook, Bloomington, IN) over a coaxial 0.014″ diameter guidewire (Prowater; Abbott Laboratories, Redwood City, CA). Under X-ray fluoroscopy, an iodinated contrast agent (Iohexol; Omnipaque 350; Amersham, Princeton, NJ) was used for DSA and a 2-F catheter (JB-1; Cook, Bloomington, IN) was used to selectively interrogate the celiac artery and advance into the hepatic artery.

IRE procedure

For IRE, each rabbit was fixed in a supine position and the left medial hepatic lobe was exposed through a mini-laparotomy incision. This lobe was gently pulled out and placed on sterile gauze using two cotton applicators. A parallel two-electrode array (diameter 0.4 mm, distance 5 or 10 mm) was inserted into the tumor to be treated, avoiding major vessels and bile ducts (C.S. and B.W., 2 years of experience). Using a BTX Electroporator (ECM830; Harvard Apparatus, Holliston, MA), 8 pulses at 2 kV were delivered with a 100 μs duration and 100 ms spacing.[20] After the IRE procedure, the abdominal incisions were closed with a two-layer technique.

MRI acquisition

MRI images were acquired using a 15-channel knee coil on a 3T clinical unit (Magnetom Skyra; Siemens Medical Solutions, Erlangen, Germany) before and immediately after IRE treatment. The baseline protocol included axial T1-weighted gradient-echo and axial respiration-triggered T2-weighted spin-echo sequences and was used to plan the IRE intervention. In the post-treatment scan session, these two sequences were repeated, and a dynamic contrast-enhanced protocol was applied for TRIP-MRI, consisting of continuous repetitions of a spoiled gradient-echo T1-weighted sequence for a total of about 11 minutes; after one minute of scanning, 3 mL of 5% gadopentetate dimeglumine solution (Magnevist; Bayer Schering Pharma, Whippany, NJ) was administered over 5 seconds, followed by the same amount of saline solution.[17–19] Finally, the T1-weighted sequence was repeated once more to evaluate late contrast enhancement. The acquisition parameters for each sequence are reported in Table 1. Due to the time needed for closing the abdominal incision, moving the rabbit to the MRI room and scanning the anatomical images, the TRIP-MRI was started approximately 30 minutes after IRE on average.

MRI analysis

The area of the necrotic center and enhancing boundary was measured for each treated tumor on a single slice of the post-contrast T1-weighted image based on contrast enhancement. We assumed these to correspond to the IRE and RE zone respectively; this hypothesis was validated by visual comparison with histology and correlation between the area measurements obtained by the two modalities. On the basis of pre- and post-IRE T1W, T2W, contrast-enhanced T1W images, and TRIPMR images, tumor region of interest (ROI) and ROI of IRE zone (RE zone between tumor ROI and IRE ROI) were drawn on perfusion maps for each tumor by consensus of two experienced radiologists (LP and SH, more than 6 years' experience reading abdominal MRI and 2 years' experience of pre-clinical VX2 liver IRE research) under the instruction of an senior radiologist (ZZ, more than 15 years' experience reading abdominal MRI).

IRE zone and RE zone of the IRE treated tumor, untreated tumor (if present), right and left lobe of the healthy liver. Their average size was 198 mm^3 for the IRE zone, 211 mm^3 for the RE zone, 604 mm^3 for untreated tumors and 340 mm^3 for the healthy liver. The healthy liver ROIs were drawn as far as possible from the treated areas and from large vessels; imaging artifacts were carefully excluded in all the remaining ROIs. 14 ROIs in IRE zone of the treated tumor, 12 ROIs in RE zone, 7 ROIs in untreated tumors and 10 ROIs in each liver lobe were included for the subsequent analysis. All the ROIs for area measurements and perfusion analysis were manually drawn using ITK-SNAP version 3.6 [21]

Time-intensity curves were plotted for each ROI after smoothing with a moving-average filter, and the time and signal intensity were registered from 5 points that were manually selected as in Supporting Information Figure S1: baseline (1), contrast arrival (2), end of the initial linear signal increase (3), peak or beginning of the final plateau (4), end (5). Each curve was normalized in order to obtain the relative variation with respect to the baseline signal intensity, and 5 parameters were calculated according to the formulas in Supporting Information Figure S1: time to peak (TTP), maximum enhancement (ME), wash-in rate

(WIR), late enhancement (LE), wash-out rate (WOR). When the maximum enhancement was less than 5% of the baseline value (SI_1 in Supporting Information Figure S1), all the other parameters were not evaluated. Additionally, the minimum interval between the time of contrast arrival and the end of the acquisition was calculated among all the ROIs, and the area under the curve (AUC) was calculated for the resulting duration from the time of contrast arrival. All the signal processing and analysis were performed in Matlab® R2016a (Mathworks, Natick, MA).

Histology

After the post-IRE MRI scan, the liver tissues were harvested for histological examinations. Two to three sections across the lesion were sampled and fixed in 10% formaldehyde solution. The samples were sent to Northwestern University Pathology Core Facility for hematoxylin-eosin (HE) staining to assess both tumor IRE and RE zones, terminal deoxynucleotidyl transferase dUTP nick end labeling (TUNEL) staining to assess cell apoptosis, and CD31 (PECAM-1(M-20):sc-1506, SANTA CRUZ BIOTECHNOLOGY) staining to assess malignant tumor neovascularization. The sections, including IRE zone, RE zone, and the surrounding untreated tumor tissue, were sampled along the MRI orientation. For the CD31 staining, tissue sections were routinely processed and subjected to antigen retrieval. After blocked with 10% BSA and horse serum in PBS for 1 h, tissue sections were incubated with the anti-CD31antibody diluted in blocking solution overnight at 4°C in a humidified chamber. Sections were washed three times with PBS, incubated with peroxidase conjugate second antibody. After washing with PBS, the sections were incubated with diaminobenzidine (DAB) substrate to stain immunolabelling and then with Mayer's hematoxylin. Upon staining process was completed, the histology slides were reviewed by a pathologist. The necrosis (IRE zone) and boundary (RE zone) were measured on HE slides, and the viable area fraction was computed as the ratio of the non-necrotic and total tumor area. Three quantitative histology measures were evaluated in the IRE zone and RE zone of treated tumors, as well as in control tumors i.e. the number of tumor cells from HE slides, the apoptosis fraction from TUNEL slides and the microvessel density from CD31 slides. The apoptotic fraction was defined as the area of apoptosis expressed as a percentage of the total tumor area. For microvessel density measurements, hot spots were identified at 200X magnification level and brownish-color endothelial cells or clusters clearly separated from other adjacent vascular structures, tumor cell, and connective tissue elements were counted at 400X magnification level.[22,23] All these three measurements were evaluated by two investigators (SH and JY, both with 5 years of experience) independently in at least 5 fields per specimen, and then averaged.

Statistical analysis

The 6 parameters extracted from the time-intensity curve were evaluated in each group of ROIs. Since no significant difference was found between the left and right lobe of the liver, all the healthy liver values for each metric were pooled together during analysis. The statistical significance of the differences between the 4 groups (tumor IRE zone, tumor RE zone, untreated tumor, and healthy liver) was evaluated via Wilcoxon rank-sum tests. A *P*-value of 0.05 after Bonferroni-Holm correction for multiple comparisons was considered significant. The same statistical analysis was performed for histology results. The correlation

between MRI and histology-based metrics was evaluated by Pearson's correlation coefficient.

Results

MRI and DSA images

Representative MRI images are shown in Figure 1A. All the tumors appeared quite consistently hyperintense on T2-weighted and hypointense on pre-contrast T1-weighted images both before and after IRE treatment, with a less homogeneous signal after IRE. The core (IRE zone) of the treated tumor on the post-contrast T1-weighted images was hypointense but a rim or a few foci with variable signal enhancement (RE zone) were observed in 15/17 rabbits. DSA confirmed the correct placement of the catheter and showed a reduction of vessels in the treated tumors (Figure 1B).

Time-intensity curves

Representative time-intensity curves for the different types of ROIs were presented in Figure 2. Corresponding histology analysis for the different types of ROIs were presented in the Supporting Information Figure S2. In IRE zone of the treated tumors, there was only a moderate and slow signal increase after the injection of the contrast agent. In RE zone of the treated tumors, the signal increased more and usually reached a plateau without decreasing until the end of the acquisition time window. In untreated tumors, the signal increased rapidly, reached a peak and then decreased. In the healthy liver, the signal increased rapidly to an intermediate level and then decreased more rapidly than in tumors.

The quantitative parameters extracted from the curves allow these differences between groups to be more systematically assessed (Figure 3). AUC was significantly lower in IRE zone of treated tumors than in RE zone of treated tumors and untreated tumors (−70% compared to both regions). Besides, AUC was higher in RE zone and untreated tumors compared to the healthy liver (+259% and +246% respectively). TTP was higher in IRE zone of the treated tumors than in RE zone of the treated tumors (+53%), untreated tumors (+210%) and liver (+468%). All the differences were significant except between RE zone of treated tumors and untreated tumors. ME was significantly lower in IRE zone of treated tumors than in RE zone of treated tumors and untreated tumors (−67% for both). It was higher in RE zone and untreated tumor compared to the healthy liver (+128% and +127%). WIR was significantly lower in IRE zone of treated tumors than in all the other regions (−66%, −69% and −53% compared to RE zone, untreated tumors, and healthy liver respectively). LE was significantly lower in IRE zone than in RE zone (−53%) of treated tumors and significantly higher in all the tumor ROIs than in the healthy liver (+143% in IRE zone, +419% in RE zone and +365% in untreated tumors). WOR was positive in IRE zone and higher than in RE zone (+742%), where it was virtually null, untreated tumors (+165%) and healthy liver (+127%), where it was negative; all the differences were significant except between RE zone and untreated tumors. The Bonferroni-Holm-corrected p-values for all the comparisons were reported in Table 2.

Histology quantitative analysis

The results of the quantitative analysis of histology data were shown as boxplots in Figure 4. The number of tumor cells was significantly lower in IRE zones than in RE zones ($p < 0.001$) and untreated tumors ($p < 0.001$). However, it was slightly but still significantly lower in RE zones than in untreated tumors ($p = 0.017$). The apoptosis fraction was significantly higher in IRE zones than in RE zones and untreated tumors ($p < 0.001$), but not significantly different between RE zones and untreated tumors. The microvessel density was significantly lower in IRE zones than in RE zones and untreated tumors ($p < 0.001$), but not significantly different between RE zones and untreated tumors.

Histology- and MRI-based measurements of necrotic and viable areas

Representative outlines of IRE zone and RE zone are shown in Figure 5, along with quantitative results. The viable fraction area was significantly lower in treated than in untreated tumors ($P < 0.001$). In treated tumors, there was a significant correlation between MRI and histology region measurements, both for IRE zone ($r = 0.948$, $P = 2.4x10^{-8}$) and for RE zone ($r = 0.951$, $P = 1.5x10^{-8}$).

Discussion

The purpose of this study was to investigate the capability of TRIP-MRI to detect perfusion alterations in liver tumors immediately after IRE ablation, particularly focusing on the differentiation of the effectively tumor IRE zone and the surrounding tumor RE zone. TRIP-MRI metrics were significantly different between IRE zone and RE zone of the treated tumor, showing a dramatic decrease of overall perfusion, a greatly decreased and delayed enhancement, and slower wash-in and wash-out in the effectively treated areas. Conversely, there was no significant difference between the boundary of the treated tumors and the untreated tumors, although a trend towards longer time-to-peak and slower wash-out could be observed.

IRE a promising treatment for patients who are not candidates for surgery and/or cannot tolerate thermal ablative techniques.[24–26] Additional advantages of IRE ablation include triggering anti-tumor specific immunological reaction [27] and having minimal impact on the tissue collagen network.[26,28] These benefits make IRE an attractive approach for the treatment of patients with unresectable HCC and metastatic liver tumors.[25,26] Recently, López-Alonso et al. differentiated RE and IRE using temporal ultrastructural changes after electroporation in pig liver.[29] Moreover, developing non-invasive imaging techniques for accurate prediction IRE zone) after-IRE procedures and early identification of inadequately treated RE zone will be critical for broad, effective clinical application.

In this study, tumor histopathology showed a significantly higher degree of apoptosis in IRE zones than in RE zones of the treated tumors and in untreated tumors. All the parameters derived from TRIP-MRI had a negative correlation with either the apoptosis fraction or the number of tumor cells, suggesting that the observed perfusion reduction was strongly associated with cell death induced by IRE treatment. On the other hand, the correlations between TRIP-MRI metrics and the microvessel density were significant but relatively low,

which is surprising because microvessel density is a direct biomarker of perfusion. A possible explanation is that CD31 staining is inherently less repeatable, so the correlations might be affected by a higher degree of experimental variability.

Our results were compatible with the qualitative imaging appearance of IRE-treated tumors in previous studies. Granata et al. showed MRI enhancement (intravenous injection) in 2 out of 24 patients with a partial response one month after IRE and no enhancement in the remaining patients with complete response.[30] Chung et al. imaged the IRE-treated normal porcine liver with computer tomography and found a central non-enhancing zone surrounded by two enhancing layers.[31] Besides, previous TRIP-MRI studies showed perfusion reduction in liver tumors after chemoembolization in patients [17,19] or after radiofrequency ablation in rabbits.[18] Our recently published data demonstrated a statistically significant Apparent Difffusion Coefficient (ADC) increase immediately after IRE of HCC in rabbits.[32] We previously showed similar results in a pancreatic tumor mouse model one day after IRE.[33] On the other hand, the only clinical study we are aware of including MRI less than one day after IRE showed a decrease in ADC.[34] This inconsistency could be due to the many factors that can lead to a change in ADC, making it very sensitive to the experimental conditions. Perfusion MRI measures should be more directly related to IRE effects, though they require contrast agent injections. Future work should compare the performance of the method proposed here with standard diffusion and perfusion MRI, which are routinely acquired in tumor patients.

Some previous TRIP-MRI studies used kinetic models to obtain parameters with a specific physiological meaning,[35] similarly to the procedure followed within dynamic contrast-enhanced MRI studies.[36] However, this approach requires measurement or estimation of the T1 values of the tissue and the arterial input function. Also, it’s sensitive to variations in the injection procedure. Therefore, we followed a semi-quantitative approach for the sake of reliability and clinical translatability.

The application of kinetic models could be investigated in the future, as well as other quantitative modalities. We focused on the immediate post-IRE time point because it has the highest clinical relevance, but further time points should be investigated in future studies. Another possible limitation of our study is the difficulty to co-localize MRI and histology data within the treated tumors; however, the significant correlation between the corresponding regions suggest that the non-enhancing and enhancing zones precisely correspond to IRE and RE areas respectively.

If the results of the present study are confirmed in a larger cohort and in patients, the translation into the interventional practice should be relatively straightforward, especially considering that the MRI acquisition and post-processing methods are very easy to implement. The only issues could be the need to perform intra-arterial catheterization with an MRI-compatible catheter and the presence of an MRI scanner within or close to the operating suite to image the patient shortly after the procedure and immediately follow-up with further interventions when needed. However, these should not be major problems in most interventional settings, and the catheter could be used also for drug delivery[37], thus improving the overall efficacy of the intervention even further.

Our results showed that TRIP-MRI can detect immediate perfusion changes in IRE-treated liver tumors and differentiate effectively IRE zone from the surrounding tumor RE zone. This approach could enable vital applications in the clinical practice, allowing timely interventions on the residual tumors and maximizing the ultimate efficacy of the treatment.

Supplementary Material

Refer to Web version on PubMed Central for supplementary material.

Acknowledgement

This work was supported by grants R01CA196967 and R01CA209886 funded by the USA National Cancer Institute (National Institutes of Health). None of the authors has any conflict of interest.

References

1. Wells SA, Hinshaw JL, Lubner MG, Ziemlewicz TJ, Brace CL, Lee FT Jr., Liver Ablation: Best Practice. Radiol Clin North Am 2015;53(5):933–971. [PubMed: 26321447]
2. Gervais DA, Goldberg SN, Brown DB, Soulen MC, Millward SF, Rajan DK, Interventional Oncology Task F, Standards Division SoIR. Society of Interventional Radiology position statement on percutaneous radiofrequency ablation for the treatment of liver tumors. J Vasc Interv Radiol 2009;20(1):3–8. [PubMed: 18948025]
3. Boas FE, Bodei L, Sofocleous CT. Radioembolization of Colorectal Liver Metastases: Indications, Technique, and Outcomes. J Nucl Med 2017;58(Suppl 2):104S–111S. [PubMed: 28864605]
4. Lencioni R, Crocetti L. Local-regional treatment of hepatocellular carcinoma. Radiology 2012;262(1):43–58. [PubMed: 22190656]
5. Davalos R, Mir L, Rubinsky B. Tissue Ablation with Irreversible Electroporation. Ann Biomed Eng 2005;33(2):223–231. [PubMed: 15771276]
6. Scheffer HJ, Nielsen K, de Jong MC, van Tilborg AAJM, Vieveen JM, Bouwman A, Meijer S, van Kuijk C, van Den Tol P, Meijerink MR. Irreversible Electroporation for Nonthermal Tumor Ablation in the Clinical Setting: A Systematic Review of Safety and Efficacy. J Vasc Interv Radiol 2014;25(7):997–1011. [PubMed: 24656178]
7. Chen X, Ren Z, Zhu T, Zhang X, Peng Z, Xie H, Zhou L, Yin S, Sun J, Zheng S. Electric Ablation with Irreversible Electroporation (IRE) in Vital Hepatic Structures and Follow-up Investigation. Sci Rep 2015;5(1).
8. Paiella S, Butturini G, Frigerio I, Salvia R, Armatura G, Bacchion M, Fontana M, D"Onofrio M, Martone E, Bassi C. Safety and Feasibility of Irreversible Electroporation (IRE) in Patients with Locally Advanced Pancreatic Cancer: Results of a Prospective Study. Dig Surg 2015;32(2):90–97. [PubMed: 25765775]
9. Rossmeisl J, Garcia PA, Pancotto T, Robertson J, Henao-Guerrero N, Neal R, Ellis T, Davalos R. Safety and feasibility of the Nano Knife system for irreversible electroporation ablative treatment of canine spontaneous intracranial gliomas. J Neurosurg 2015;123(4):1008–1025. [PubMed: 26140483]
10. Valerio M, Stricker PD, Ahmed HU, Dickinson L, Ponsky L, Shnier R, Allen C, Emberton M. Initial assessment of safety and clinical feasibility of irreversible electroporation in the focal treatment of prostate cancer. Prostate Cancer Prostatic Dis 2014;17(4).
11. Wagstaff PGK, de Bruin DM, Zondervan PJ, Savci Heijink CD, Engelbrecht MRW, van Delden OM, van Leeuwen TG, Wijkstra H, de la Rosette JJ, Laguna Pes MP. The efficacy and safety of irreversible electroporation for the ablation of renal masses: a prospective, human, in-vivo study protocol.(Clinical report). BMC Cancer 2015;15(1).
12. Ben-David E, Ahmed M, Faroja M, Moussa M, Wandel A, Sosna J, Appelbaum L, Nissenbaum I, Goldberg SN. Irreversible electroporation: treatment effect is susceptible to local environment and tissue properties. Radiology 2013;269(3):738. [PubMed: 23847254]

13. Corovic S, Lackovic I, Sustaric P, Sustar T, Rodic T, Miklavcic D. Modeling of electric field distribution in tissues during electroporation.(Report). Biomed Eng Online 2013;12(1).
14. Jiang C, Davalos RV, Bischof JC. A Review of Basic to Clinical Studies of Irreversible Electroporation Therapy. IEEE Trans Biomed Eng 2015;62(1):4–20. [PubMed: 25389236]
15. Granata V, Lutio di Castelguidone E, Fusco R, Catalano O, Piccirillo M, Palaia R, Izzo F, Gallipoli A, Petrillo A. Irreversible electroporation of hepatocellular carcinoma: preliminary report on the diagnostic accuracy of magnetic resonance, computer tomography, and contrast-enhanced ultrasound in evaluation of the ablated area. Radiol Med 2016;121(2):122–131. [PubMed: 26345332]
16. Figini M, Wang X, Lyu T, Su Z, Procissi D, Yaghmai V, Larson AC, Zhang Z. Preclinical and clinical evaluation of the liver tumor irreversible electroporation by magnetic resonance imaging. Am J Transl Res 2017;9(2):580–590. [PubMed: 28337285]
17. Wang D, Gaba RC, Jin B, Lewandowski RJ, Riaz A, Memon K, Ryu RK, Sato KT, Kulik LM, Mulcahy MF, Larson AC, Salem R, Omary RA. Perfusion reduction at transcatheter intraarterial perfusion MR imaging: a promising intraprocedural biomarker to predict transplant-free survival during chemoembolization of hepatocellular carcinoma. Radiology 2014;272(2):587–597. [PubMed: 24678859]
18. Sato KT, Wang D, Lewandowski RJ, Ryu RK, Klein RA, Salem R, Larson AC, Omary RA. Four-dimensional transcatheter intraarterial perfusion MRI monitoring of radiofrequency ablation of rabbit VX2 liver tumors. J Magn Reson Imaging 2011;34(3):563–569. [PubMed: 21761464]
19. Wang D, Gaba RC, Jin B, Riaz A, Lewandowski RJ, Ryu RK, Sato KT, Ragin AB, Kulik LM, Mulcahy MF, Salem R, Larson AC, Omary RA. Intraprocedural Transcatheter Intra-arterial Perfusion MRI as a Predictor of Tumor Response to Chemoembolization for Hepatocellular Carcinoma. Acad Radiol 2011;18(7):828–836. [PubMed: 21669349]
20. Zhang Y, White SB, Nicolai JR, Zhang Z, West DL, Kim D-H, Goodwin AL, Miller FH, Omary RA, Larson AC. Multimodality imaging to assess immediate response to irreversible electroporation in a rat liver tumor model. Radiology 2014;271(3):721. [PubMed: 24555632]
21. Yushkevich PA, Piven J, Hazlett HC, Smith RG, Ho S, Gee JC, Gerig G. User-guided 3D active contour segmentation of anatomical structures: Significantly improved efficiency and reliability. NeuroImage 2006;31(3):1116–1128. [PubMed: 16545965]
22. Weidner N, Folkman MJ, Pozza F, Bevilacqua P, Allred EN, Moore DH, Meli S, Gasparini G. Tumor angiogenesis: a new significant and independent prognostic indicator in early-stage breast carcinoma. J Natl Cancer Inst 1992;84(24):1875. [PubMed: 1281237]
23. Mineo TC, Ambrogi V, Baldi A, Rabitti C, Bollero P, Vincenzi B, Tonini G. Prognostic impact of VEGF, CD31, CD34, and CD105 expression and tumour vessel invasion after radical surgery for IB–IIA non-small cell lung cancer. J Clin Pathol 2004;57(6):591. [PubMed: 15166262]
24. Lee YJ, Lu DS, Osuagwu F, Lassman C. Irreversible electroporation in porcine liver: short- and long-term effect on the hepatic veins and adjacent tissue by CT with pathological correlation. Invest Radiol 2012;47(11):671–675. [PubMed: 23037001]
25. Distelmaier M, Barabasch A, Heil P, Kraemer NA, Isfort P, Keil S, Kuhl CK, Bruners P. Midterm Safety and Efficacy of Irreversible Electroporation of Malignant Liver Tumors Located Close to Major Portal or Hepatic Veins. Radiology 2017;285(3):1023–1031. [PubMed: 28799842]
26. Sutter O, Calvo J, N'Kontchou G, Nault JC, Ourabia R, Nahon P, Ganne-Carrie N, Bourcier V, Zentar N, Bouhafs F, Sellier N, Diallo A, Seror O. Safety and Efficacy of Irreversible Electroporation for the Treatment of Hepatocellular Carcinoma Not Amenable to Thermal Ablation Techniques: A Retrospective Single-Center Case Series. Radiology 2017;284(3):877–886. [PubMed: 28453431]
27. Al-Sakere B, Bernat C, Andre F, Connault E, Opolon P, Davalos RV, Mir LM. A study of the immunological response to tumor ablation with irreversible electroporation. Technol Cancer Res Treat 2007;6(4):301–306. [PubMed: 17668937]
28. Maor E, Ivorra A, Leor J, Rubinsky B. The effect of irreversible electroporation on blood vessels. Technol Cancer Res Treat 2007;6(4):307–312. [PubMed: 17668938]
29. López-Alonso B, Hernáez A, Sarnago H, Naval A, Güemes A, Junquera C, Burdío JM, Castiella T, Monleón E, Gracia-Llanes J, Burdio F, Mejía E, Lucía O. Histopathological and Ultrastructural

Changes after Electroporation in Pig Liver Using Parallel-Plate Electrodes and High-Performance Generator. Scientific Reports 2019;9(1):2647. [PubMed: 30804395]

30. Granata V, Fusco R, Catalano O, Piccirillo M, De Bellis M, Izzo F, Petrillo A. Percutaneous ablation therapy of hepatocellular carcinoma with irreversible electroporation: MRI findings. AJR Am J Roentgenol 2015;204(5):1000. [PubMed: 25905934]
31. Chung DJ, Sung K, Osuagwu FC, Wu HH, Lassman C, Lu DSK. Contrast Enhancement Patterns after Irreversible Electroporation: Experimental Study of CT Perfusion Correlated to Histopathology in Normal Porcine Liver. J Vasc Interv Radiol 2016;27(1):104–111. [PubMed: 26547121]
32. Hu S, Sun C, Wang B, Zhou K, Pan L, Shangguan J, Yang J, Yaghmai V, Figini M, Zhang Z. Diffusion-Weighted MR Imaging to Evaluate Immediate Response to Irreversible Electroporation in a Rabbit VX2 Liver Tumor Model. J Vasc Interv Radiol 2019;30(11):1863–1869. [PubMed: 31542271]
33. Figini M, Wang X, Lyu T, Su Z, Wang B, Sun C, Shangguan J, Pan L, Zhou K, Ma Q, Yaghmai V, Procissi D, Larson AC, Zhang Z. Diffusion MRI biomarkers predict the outcome of irreversible electroporation in a pancreatic tumor mouse model. Am J Cancer Res 2018;8(8):1615–1623. [PubMed: 30210929]
34. Barabasch A, Distelmaier M, Heil P, Kramer NA, Kuhl CK, Bruners P. Magnetic Resonance Imaging Findings After Percutaneous Irreversible Electroporation of Liver Metastases: A Systematic Longitudinal Study. Invest Radiol 2017;52(1):23–29. [PubMed: 27379698]
35. Wang D, Jin B, Lewandowski RJ, Ryu RK, Sato KT, Mulcahy MF, Kulik LM, Miller FH, Salem R, Li D, Omary RA, Larson AC. Quantitative 4D transcatheter intraarterial perfusion MRI for monitoring chemoembolization of hepatocellular carcinoma. J Magn Reson Imaging 2010;31(5):1106–1116. [PubMed: 20432345]
36. Sourbron SP, Buckley DL. Classic models for dynamic contrast-enhanced MRI. NMR Biomed 2013;26(8):1004–1027. [PubMed: 23674304]
37. Bhutiani N, Agle S, Li Y, Li S, Martin RCG II. Irreversible electroporation enhances delivery of gemcitabine to pancreatic adenocarcinoma. Journal of Surgical Oncology 2016;114(2):181–186. [PubMed: 27393627]

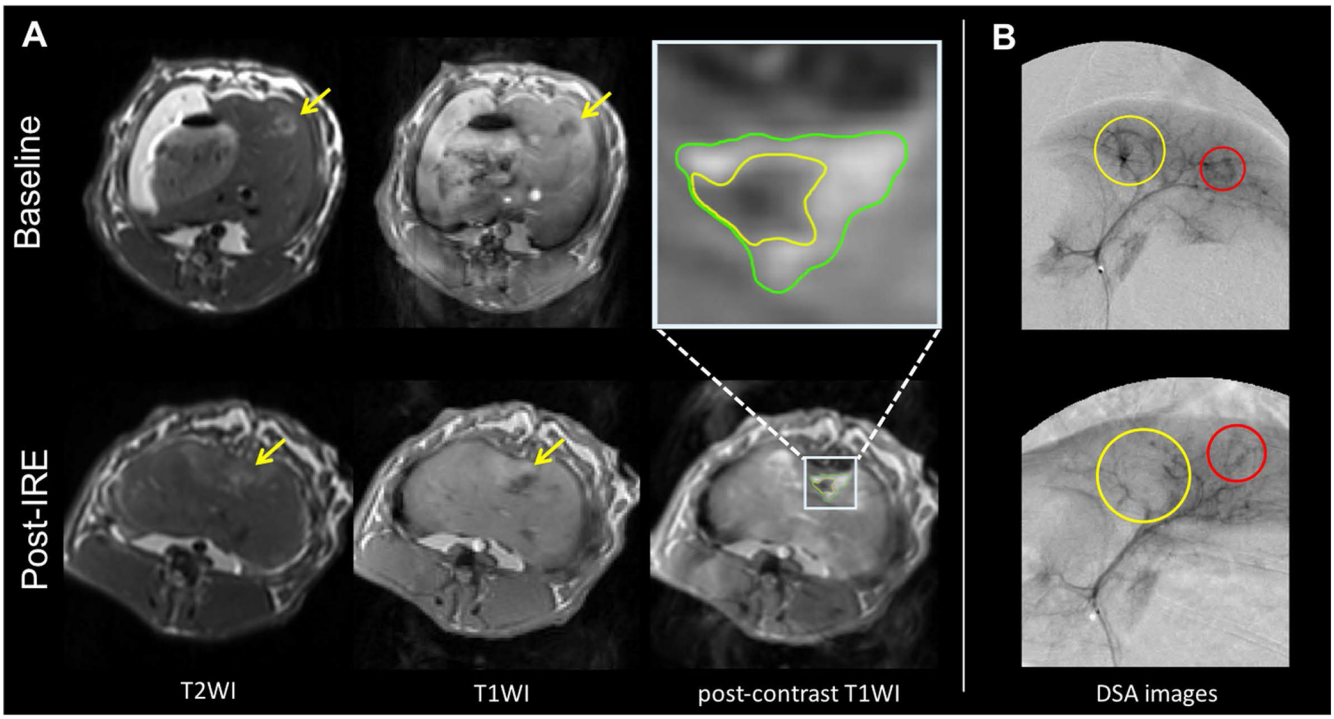

Figure 1:
Representative MRI and DSA images. A, On T2-weighted MRI images (left) the tumor (yellow arrow) is hyperintense, with less homogeneous signal after treatment. On T1-weighted images (second and third column) it is hypointense, with a boundary (RE zone) of contrast enhancement after treatment. B, DSA images (right) show an almost complete absence of vessels in the treated tumor (yellow circle) after IRE treatment, whereas vessels are preserved in the untreated tumor (red circle).

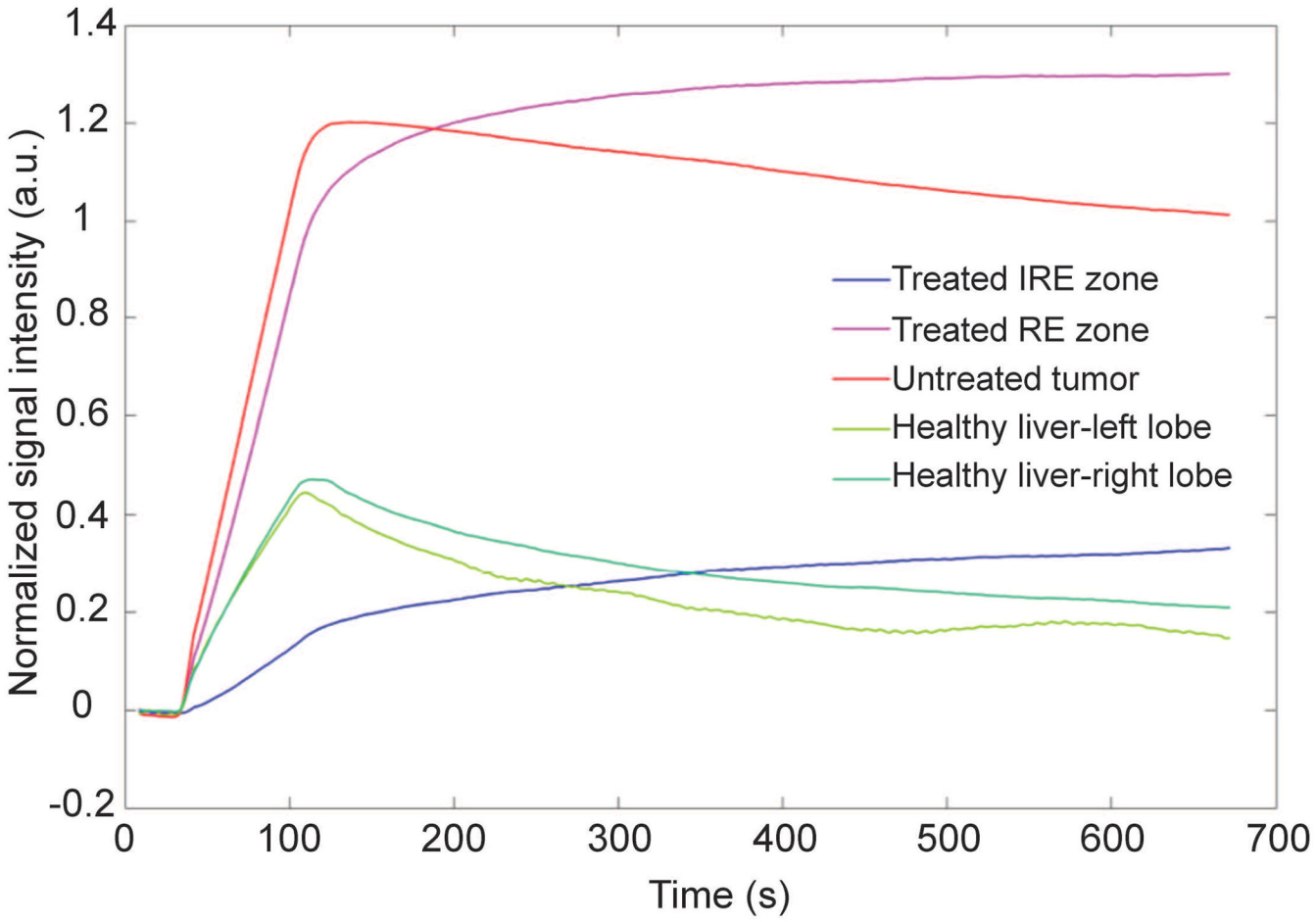

Figure 2:

Representative time-intensity curves in the 5 ROIs of one rabbit are shown on the left. In the treated tumor center (IRE zone, blue), contrast enhancement is moderate and slow, while it is higher in the boundary (RE zone, magenta) and untreated tumor (red), with the former showing no wash-out compared to the latter. Healthy liver tissues (green) show intermediate enhancement, with a peak followed by relatively rapid signal decrease.

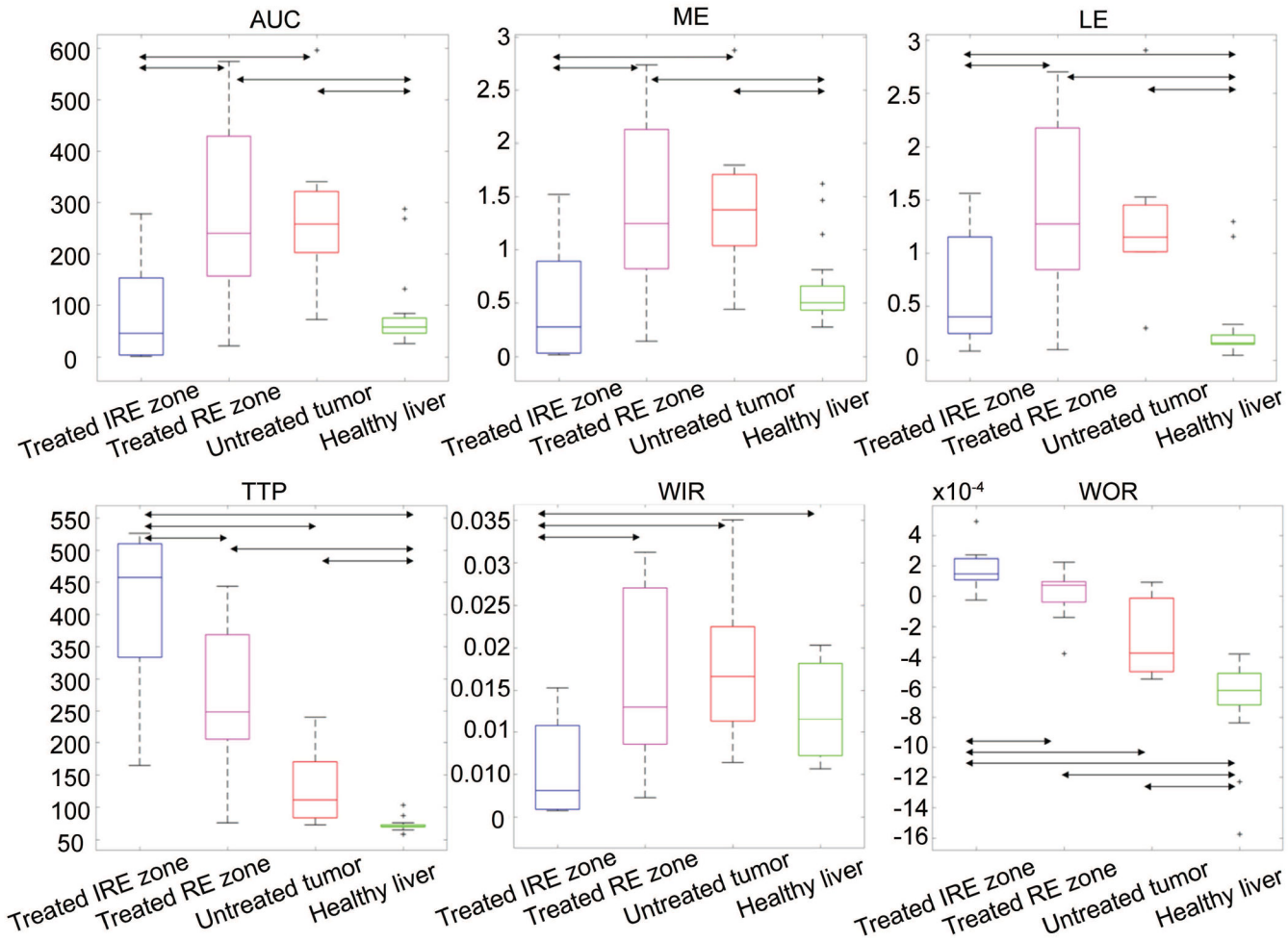

Figure 3:

MRI perfusion measurements. Boxplots for the 6 parameters (AUC, TTP, ME, WIR, LE, and WOR) extracted from the time-intensity curves in the 4 groups of ROIs (treated tumors center-IRE zone, treated tumors boundary-RE zone, untreated tumors and healthy liver). Double arrows mark significant differences.

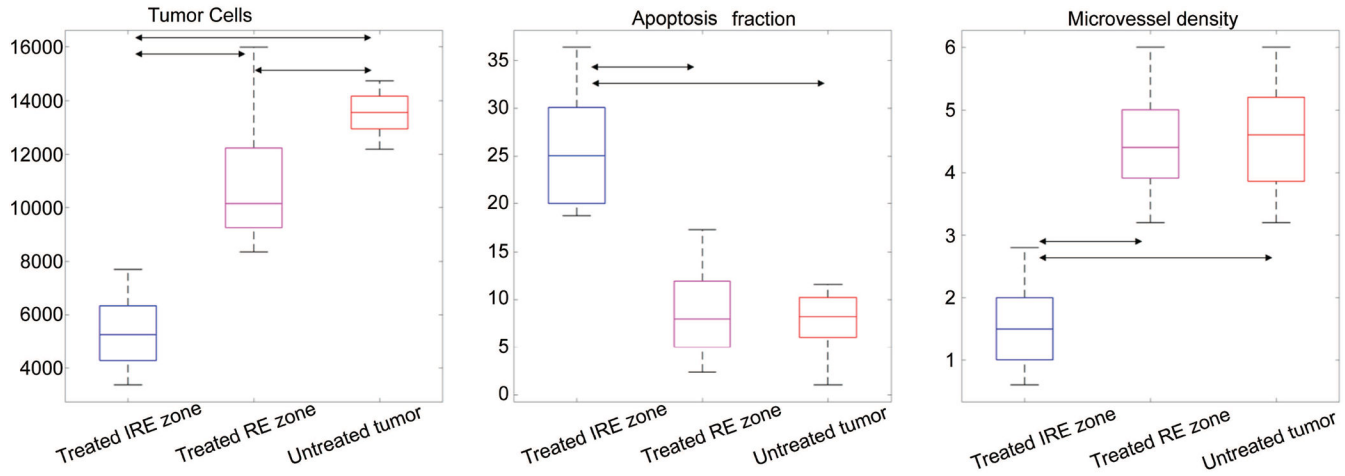

Figure 4:

Quantitative histology measurements. Boxplots for the 3 quantitative histology parameters (number of tumor cells, apoptosis fraction and microvessel density) extracted from the time-intensity curves in IRE zone of treated tumors, RE zone of treated tumors, and untreated tumors. Double arrows mark significant differences.

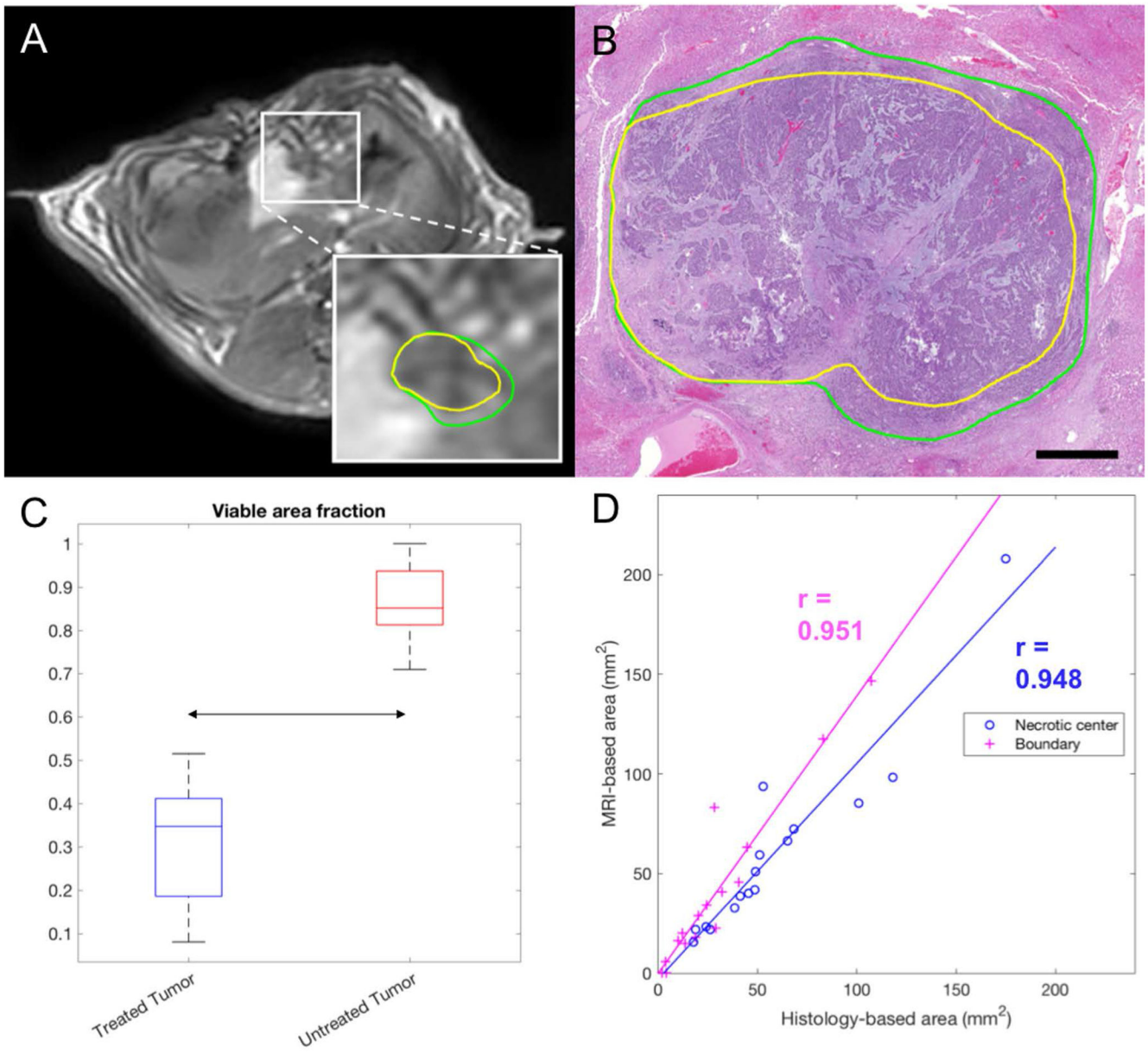

Figure 5:

MRI- and histology-based IRE and RE areas. A, Representative post-contrast T1-weighted MRI. The box shows an enlargement of the tumor area with the necrotic center (IRE zone) delineated in yellow and the enhancing rim delineated in green. B, Corresponding HE slide, with the necrotic center delineated in yellow and the enhancing rim delineated in green (RE zone). C, Boxplot for the viable area fraction measured on MRI (ratio between enhancing and total tumor area) in treated and untreated tumors. D, Correlation between the histology-based and MRI-based areas, for the IRE zone (blue) and RE zone (magenta) of the treated tumors. The regression lines and Pearson's correlation coefficients are also overlaid.

Table 1.

MRI acquisition parameters

Sequence	T2W	T1W	TRIP
Purpose	Turbo spin-echo anatomy (pre- and post-IRE)	Gradient-echo anatomy (pre- and post-IRE) and late enhancement (post IRE)	Spoiled gradient-echo perfusion evaluation (post-IRE)
Repetition time	4000 ms	200 ms	2.6 ms
Echo time	39 ms	2.93 ms	1.02 ms
Flip angle	150°	70°	8°
Field of view	180x180 mm^2	180x180 mm^2	128x112 mm^2
Slices	17	17	20
Voxel size	0.47x0.47x2 mm^3	0.8x0.8x2 mm^3	1x1x2 mm^3

Table 2.

Bonferroni-Holm-corrected p-values for all the comparisons among different regions (treated tumor center, treated tumor boundary, untreated tumor, healthy liver) for all the TRIP-MRI semi-quantitative parameters (AUC = area under the curve; TTP = time-to-peak, ME = maximum enhancement, WIR = wash-in rate, LE = late enhancement, WOR = wash-out rate). The significant differences ($P < 0.05$) are marked by asterisks.

	AUC	TTP	ME	WIR	LE	WOR
Treated center vs treated boundary	0.019*	0.045*	0.019*	0.040*	0.032*	0.045*
Treated center vs untreated tumor	0.019*	0.002*	0.019*	0.019*	0.133	0.002*
Treated center vs healthy liver	0.286	<0.001*	0.069	0.040*	0.040*	<0.001*
Treated boundary vs untreated tumor	1.000	0.078	1.000	1.000	1.000	0.179
Treated boundary vs healthy liver	0.002*	<0.001*	0.005*	0.284	0.001*	<0.001*
Untreated tumor vs healthy liver	0.007*	0.004*	0.024*	0.103	0.006*	0.007*